Hydrodynamics of microbial filter feeding

Lasse Tor Nielsen[a,1], Seyed Saeed Asadzadeh[b], Julia Dölger[c], Jens H. Walther[b,d], Thomas Kiørboe[a], and Anders Andersen[c]

[a]National Institute of Aquatic Resources and Centre for Ocean Life, Technical University of Denmark, DK-2800 Kongens Lyngby, Denmark; [b]Department of Mechanical Engineering, Technical University of Denmark, DK-2800 Kongens Lyngby, Denmark; [c]Department of Physics and Centre for Ocean Life, Technical University of Denmark, DK-2800 Kongens Lyngby, Denmark; and [d]Swiss Federal Institute of Technology Zürich, Chair of Computational Science, ETH Zentrum, CH-8092 Zürich, Switzerland

Edited by M. A. R. Koehl, University of California, Berkeley, CA, and approved July 10, 2017 (received for review June 7, 2017)

Microbial filter feeders are an important group of grazers, significant to the microbial loop, aquatic food webs, and biogeochemical cycling. Our understanding of microbial filter feeding is poor, and, importantly, it is unknown what force microbial filter feeders must generate to process adequate amounts of water. Also, the trade-off in the filter spacing remains unexplored, despite its simple formulation: A filter too coarse will allow suitably sized prey to pass unintercepted, whereas a filter too fine will cause strong flow resistance. We quantify the feeding flow of the filter-feeding choanoflagellate *Diaphanoeca grandis* using particle tracking, and demonstrate that the current understanding of microbial filter feeding is inconsistent with computational fluid dynamics (CFD) and analytical estimates. Both approaches underestimate observed filtration rates by more than an order of magnitude; the beating flagellum is simply unable to draw enough water through the fine filter. We find similar discrepancies for other choanoflagellate species, highlighting an apparent paradox. Our observations motivate us to suggest a radically different filtration mechanism that requires a flagellar vane (sheet), something notoriously difficult to visualize but sporadically observed in the related choanocytes (sponges). A CFD model with a flagellar vane correctly predicts the filtration rate of *D. grandis*, and using a simple model we can account for the filtration rates of other microbial filter feeders. We finally predict how optimum filter mesh size increases with cell size in microbial filter feeders, a prediction that accords very well with observations. We expect our results to be of significance for small-scale biophysics and trait-based ecological modeling.

protozoans | choanoflagellates | filter feeding | microswimmers | computational fluid dynamics

Heterotrophic microorganisms in the oceans inhabit a dilute environment and they need efficient feeding mechanisms to acquire enough food to sustain growth (1, 2). At the microscale the Reynolds number is low and viscous forces govern hydrodynamical interactions. This implies extensive, long-range flow disturbances around moving particles and microswimmers, impeding cell–cell contact and prey capture (3, 4). However, to encounter enough food, purely heterotrophic plankton that rely solely on prey capture typically need to clear a volume of water for prey corresponding to 1 million times their own body volume per day (4). Thus, heterotrophic microbes face a difficult challenge, and the prevailing viscous forces must strongly influence prey capture and shape the various feeding modes through evolution.

Many unicellular flagellates as well as colonial sponges and metazoans, e.g., tunicates, use filter feeding to catch bacteria-sized prey (1, 5–7). They establish a feeding current, from which prey particles are sieved using filter structures. Such filter feeders benefit from having filters with small mesh size that allow the organisms to capture small prey (5, 8). However, filter spacing involves a trade-off: The finer the mesh size is, the higher the availability of food but the lower the clearance rate due to a dramatic decrease in filter permeability (9). An optimum mesh size must therefore exist. While microbial filter feeding has been studied regarding the pressure drop across the filter and the observed clearance rates (5), clearance rates have never been related to the force production of the flagellum that drives the feeding current. Can a beating flagellum even produce sufficient force to account for the observed clearance rates through such fine filters?

Choanoflagellates are the prime example of unicellular filter feeders (1, 10, 11). They are equipped with a single flagellum that is surrounded by a funnel-shaped collar filter made up of microvilli extending from the cell. Some species are sessile and attach with a stalk to solid surfaces whereas others are freely swimming and have a basket-like structure (lorica) that surrounds cell, flagellum, and filter (Fig. 1). The beating flagellum creates a feeding current that transports bacteria-sized prey to the outside of the collar filter from where the prey are transported to the cell surface and phagocytosed (10, 12–16). Far-field flows created by choanoflagellates have recently been measured and modeled for the sessile choanoflagellate *Salpingoeca rosetta* (14). However, the essential near-cell feeding flow in choanoflagellates is poorly understood and has not been resolved quantitatively in experiments (10, 11).

As a model organism of microbial filter feeders, we focus on the choanoflagellate *Diaphanoeca grandis* that swims freely and carries a lorica (Fig. 1). The lower part of the lorica has large openings, whereas the upper part is covered by a fine web with small pore sizes (13). The collar filter therefore supposedly functions as an internal filter, and prey particles should not circumvent the filter once inside the lorica.

Using *D. grandis*, we here ask: What are the mechanisms of particle capture in choanoflagellates, and what is the optimum filter spacing? We use high-speed videography and particle tracking to quantify the feeding flow. For comparison, we use

Significance

Microbes compose the majority of life in aquatic ecosystems and are crucial to the transfer of energy to higher trophic levels and to global biogeochemical cycles. They have evolved different foraging mechanisms of which our understanding is poor. Here, we demonstrate for filter-feeding choanoflagellates—the closest relatives to multicellular life—how the observed feeding flow is inconsistent with hydrodynamic theory based on the current understanding of the morphology. Instead, we argue for the widespread presence of flagellar vanes and suggest an alternative pumping mechanism. We also demonstrate a trade-off in filter spacing that allows us to predict choanoflagellate prey sizes. These mechanistic insights are important to correctly understand and model microbial heterotrophs in marine food webs.

Author contributions: L.T.N., T.K., and A.A. designed research; L.T.N. performed experiments; L.T.N. and A.A. analyzed data; S.S.A. and J.H.W. conducted CFD simulations; J.D. and A.A. developed and applied theory; and L.T.N., T.K., and A.A. wrote the paper with comments from S.S.A., J.D., and J.H.W.

The authors declare no conflict of interest.

This article is a PNAS Direct Submission.

[1]To whom correspondence should be addressed. Email: ltor@aqua.dtu.dk.

This article contains supporting information online at www.pnas.org/lookup/suppl/doi:10.1073/pnas.1708873114/-/DCSupplemental.

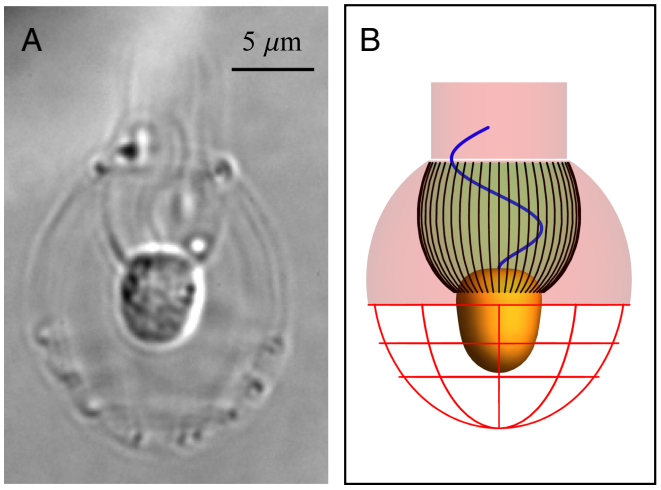

Fig. 1. Morphology of *D. grandis*. (*A*) Microscopic image of freely swimming choanoflagellate. (*B*) Model morphology with cell (orange), collar filter (green surface and black lines), flagellum (blue), and lorica (red). The ribs (costae) in the lower (posterior) part of the lorica are indicated, whereas for clarity the ribs in the finely netted, upper (anterior) part of the lorica are not shown.

computational fluid dynamic (CFD) simulations and simple estimates of the filter resistance and the force production due to the beating flagellum. Our analysis shows that modeling the beating flagellum as a simple, slender structure produces a force that is an order of magnitude too small to account for the observed clearance rate. This demonstrates the strong trade-off in small-scale filter feeding and leads us to suggest an alternative flagellar pumping mechanism.

Results

Observed Feeding Flow and Clearance Rate. We developed a generic model morphology of *D. grandis* to collate particle track observations from individual cells (*Model Morphology and Observed Flow*, Table S1, and Fig. 1). The feeding flow is driven by the beating flagellum. The flow transports particles from the region below the choanoflagellate, in through the large openings in the lower part of the lorica and up toward the collar filter on which the particles are caught (Fig. 2 and Movie S1). The detailed visualization reveals a true filtration flow that undoubtedly passes through the filter, confirming the current understanding of filter feeding in choanoflagellates (11). However, our results are for a loricate species, and it is uncertain whether, and to what extent, nonloricate species can filter the same way, since flow could pass along the filter on the outside and circumvent the filter. From the flow field, one important function of the lorica seems to be the separation of in- and exhalent flow, reducing refiltration. The clearance rate Q can be expressed as the volume flow rate through the filter

$$Q = \int_{A_F} v \, \mathrm{d}A, \qquad [1]$$

where A_F is the surface area of the filter and v is the normal component of the flow velocity. The observed velocity field shows that the water that passes the filter first passes the equator ($z = 0$) in the annular region between the cell and the finely netted part of the lorica. We determine the clearance rate as the volume flow rate upward across the annular region in the equator plane. This procedure is more precise than directly using the flow through the filter. No-slip boundary conditions would suggest reduced flow velocities near the cell and lorica. At the spatial resolution of our experiment, however, the z components of the flow velocities in the annular region do not depend on the distance from the longitudinal axis (Fig. S1*A*). To determine the clearance rate we therefore use the average value $v_z = 7.3 \pm 4.4$ μm·s^{-1} (mean ± SD) times the area of the annular region. We find $Q = (1.22 \pm 0.72) \cdot 10^3$ μm^3·s^{-1}, or 1.20 million cell volumes per day, where the cell volume $V_C = 88$ μm^3. The corresponding flagellar beat frequency is $f = 7.3 \pm 2.6$ Hz (Fig. S1*B*).

Computational Fluid Dynamics and Theoretical Clearance. To explore the feeding flow theoretically we numerically solve the Navier–Stokes equation and the equation of continuity for the incompressible Newtonian flow due to the beating flagellum with the known morphology (*CFD Simulations* and Figs. S2–S5). The collar filter consists of ∼50 evenly distributed microvilli (13), with a fairly uniform filter spacing and permeability along most of their length (Fig. 1). The finely netted upper part of the lorica has pore sizes in the range 0.05−0.5 μm (13), and for simplicity we treat it as an impermeable, rigid surface and neglect the ribs in the lower part of the lorica. *D. grandis* carries a standard eukaryotic flagellum with diameter $b = 0.3$ μm (23), and high-speed videography showed that the flagellum beats, like most other eukaryotic flagella, in a single plane (Movie S2). For computational simplicity we model the flagellum as a thin sheet of width b that is oriented perpendicular to the plane of beating and moving with a simple traveling wave motion in the positive z direction. Based on our validation of the CFD simulations, we estimate that this approach underestimates the flagellar forces by ∼20% (Tables S2 and S3). The time-averaged CFD flow is an order of magnitude weaker than the flow observed experimentally for *D. grandis* (Fig. 2). The model leads to the time-averaged flagellum force in the z-direction $F_{0.3} = 1.1$ pN, the time-averaged power $P_{0.3} = 0.31$ fW, and the clearance rate $Q_{0.3} = 95$ μm^3·s^{-1}, which is ∼13 times lower than the clearance rate based on the observed flow field.

To generalize our CFD results and roughly estimate the clearance rates of other species of choanoflagellates, we model filter resistance and flagellum force. We describe the filter locally as a row of parallel and equidistantly spaced solid cylinders, and we model the flow far from the filter as uniform and perpendicular to the filter plane. For such simple filters we can express the flow speed through the filter

$$v = \kappa \frac{a}{\mu} \Delta p, \qquad [2]$$

where Δp is the pressure drop across the filter, κ the dimensionless permeability of the filter, and μ the dynamic viscosity. The dimensionless permeability κ is a function only of the dimensionless filter spacing l/a. We model κ by combining previous theoretical work on closely and distantly spaced filter structures, respectively (24, 25). The dimensionless permeability κ increases strongly with l/a and contributes to the filter spacing trade-off as discussed above (Fig. S6). For the model morphology we find the average dimensionless permeability $\langle \kappa \rangle = 0.41$. With a flagellum of length L and diameter b we can estimate the flagellum force

$$F_T = C_F \mu L U = 4 C_F \mu L A f, \qquad [3]$$

where C_F is the drag coefficient, $\mu = 1.0 \cdot 10^{-3}$ Pa·s the viscosity, and A the amplitude of the flagellar beat. The average speed of the flagellum is estimated as $U = 4Af$. For simplicity we take C_F to be the drag coefficient of a slender spheroid that is moving sideways, $C_F = 4\pi/(\ln(2L/b) + 1/2)$ (26). The estimate neglects the presence of filter and lorica structures surrounding the flagellum and assumes that all (primarily transversal) drag on the flagellum is converted into longitudinal flow. The corresponding power estimate is $P_T = F_T U = 16 C_F \mu L A^2 f^2$. To estimate the theoretical clearance rate we assume that the pressure drop is $\Delta p = F/A_F$ and we obtain

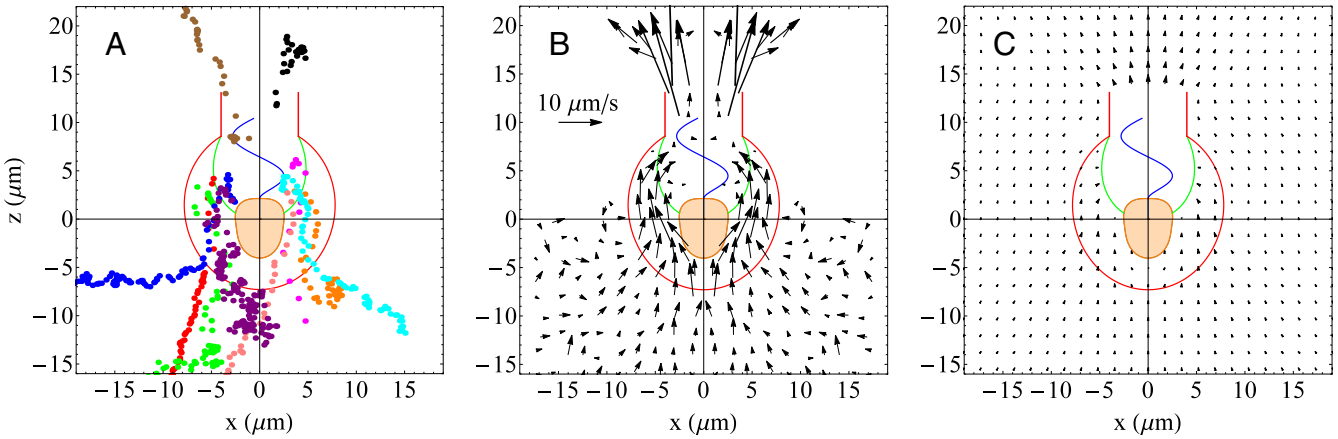

Fig. 2. Observed feeding flow generated by *D. grandis* and velocity field from CFD model based on the standard description of morphology and flagellum. The model morphology shows the cell (orange), the collar filter (green), the flagellum (blue), and the lorica (red). (*A*) Representative particle tracks. The 10 different colors correspond to 10 discrete tracks and the solid circles show particle positions with 0.1-s time intervals. The particles below the choanoflagellate move randomly due to Brownian motion and display a slow net flow toward the lorica openings. (*B*) Average velocity field based on particle tracking. The flow velocities increase dramatically as the particles enter the lorica and approach the collar filter where the particles are eventually caught. The filtered water is expelled in a concentrated jet flow upward and out of the "chimney" of the lorica opposite to and clearly separated from the intake region. (*C*) The CFD velocity field in the *xz* plane is time averaged over the flagellar beat cycle, and the velocity vectors "inside" filter and chimney are omitted for clarity. The CFD model based on the standard description of morphology and flagellum predicts a feeding flow that is more than an order of magnitude weaker than the experimentally observed flow, and it cannot account for the observed clearance rate.

$$Q_T = \langle\kappa\rangle \frac{a}{\mu} F_T = 4\langle\kappa\rangle C_F a L A f. \quad [4]$$

For *D. grandis* the estimate predicts the flagellum force $F_T = 2.5 \pm 0.9$ pN, the power $P_T = 0.20 \pm 0.14$ fW, and the clearance rate $Q_T = 75 \pm 26$ μm^3·s^{-1} in rough agreement with the CFD results.

For other choanoflagellate species we calculate the clearance rate from the analytical estimate (Eq. **4**) and compare it with observations (Table 1). In most species, the theoretical clearance rate grossly underestimates the realized, and only two species seem able to filter significant volumes of water. Of the species listed, only *D. grandis* and *Stephanoeca diplocostata* carry a lorica. The rest are nonloricate and potentially subject to filter circumvention, which we did not account for. Filter circumvention would increase the flow rate, but potentially reduce the clearance rate, since water would not actually be filtered.

Discussion

The Filter-Feeder Paradox. Our results reveal a paradox: The CFD model and the simple estimates underestimate the clearance rate based on the observed flow field by more than an order of magnitude. The flow-field–derived clearance rate seems robust, as it is similar to an earlier observation (13) and at the same time consistent with the general notion that heterotrophic plankton need to daily clear a volume of approximately 1 million times their own body volume (4). Instead, the theory can of course

Table 1. Characteristic morphological and kinematic parameters for selected choanoflagellate and choanocyte species

Species	ESR, μm	*L*, μm	*f*, Hz	*A*, μm	λ, μm	*a*, μm	*l*, μm	*W*, μm	Q_T, μm^3·s^{-1}	Q_V, μm^3·s^{-1}	*Q*, μm^3·s^{-1}	Source
*Codosiga botrytis**	3.75	29.0	30.0	6.4†	17.5	0.088	0.25	10.3†	64	34,600	2,600‡	(17, 18)
*Codosiga gracilis**	1.84	8.3	10.0	1.5§	10.3	0.075	0.54	5.5§	42	850	1,000	(10, 19)
Diaphanoeca grandis¶	2.50	11.0	10.0	4.0	10.0	0.075	0.40	8.0	65	3,200	4,400	(13)
Diaphanoeca grandis¶	2.80	11.7	7.3	2.8	8.6	0.075	0.54	8.0	75	1,410	1,220	This study
*Monosiga brevicollis**	2.00#	13.8#	50.0	2.4	12.2	0.055	0.45	6.6	476	9660	400‡	(20)
*Monosiga ovata**	1.26	6.0	14.4	2.0‖	18.5‖	0.100	0.28	4.4‖	3	2,340	1,800	(21, 22)
*Monosiga sp.**	1.63	5.5	32.5	1.0	6.0	0.100	0.50	2.5	35	490	600	(1)
*Salpingoeca amphoridium**	2.30	20.7	17.0	3.0§	17.9	0.050	0.70	3.8§	716	3,470	600‡	(10)
Stephanoeca diplocostata¶	1.80	8.3	10.0	2.0§	8.6	0.075	0.47	5.4§	40	930	4,400	(10, 19)
*Spongilla lacustris***	2.00‖	10.4	11.0	1.5‖	12.2	0.060	0.18	3.1	2	620	400‡	(20)

ESR, equivalent spherical radius of cell; *L*, flagellum length; *f*, flagellum beat frequency; *A*, amplitude of flagellar beat; λ, flagellar wavelength; *a*, microvillum radius; *l*, distance between centers of neighboring microvilli; *W*, diameter of chimney or anterior filter exhaust opening; Q_T, theoretical estimate of clearance rate based on Eq. **4**; Q_V, clearance rate estimate based on the presence of a vane according to Eq. **5**; and *Q*, observed clearance rate from incubation experiments or similar.

*Sessile.

†Estimated from ref. 18.

‡Data on *Q* were unavailable, and instead *Q* was estimated as 1 million cell volumes per day (4). In species with different morphotypes, data are for single, sessile cells.

§Estimated from ref. 10.

¶Loricate, freely swimming.

#Measured using original videos kindly provided by Mah et al. (20).

‖Estimated from ref. 21.

**Choanocyte.

be questioned, most obviously perhaps through the notion that various types of flagellar hairs often line eukaryotic flagella and could increase the force output of the flagellum (23). However, the force estimate is only weakly influenced by the flagellum diameter (Eq. **3**), as long as we neglect interaction between flagellum and filter, and simple flagellar hairs would have little influence on the clearance rate. It is thus difficult to see how the flagellum would be able to deliver the force required to account for the experimentally observed clearance rate, unless some major aspect of its morphology or function has been overlooked.

Pumping Mechanism Conjecture. A few choanoflagellate species have been shown to have a so-called flagellar vane composed of a sheet-like structure along the length of the flagellum (17, 20, 27). Although a flagellar vane has been observed in a few choanoflagellate species, the structure remains elusive. Leadbeater (27) went so far as to call it a "mystery" because the structure is notoriously difficult to visualize using electron microscopy. While a vane cannot account for the clearance rate due to increased flagellum drag as long as interactions between flagellum and filter are neglected, this structure could still offer a satisfactory solution to the apparent paradox: With a vane, the distance between flagellum and the inside of the collar would be reduced, reducing transversal flow past the beating flagellum inside the collar. Instead, more fluid would be forced upward, and the resulting low pressure would have to be equalized by a flux through the filter. With a flagellar vane nearly as wide as the collar, or even physically attached to the inside of the collar, the pumping mechanism would be radically different. The highly similar choanocytes of aquatic sponges have been shown to have flagellar vanes that indeed are attached to the filter or span its width (20, 28, 29). The flagellum together with its vane would function as a waving wall forming two adjacent peristaltic pumps (30), one on each side of the vane, that draw in water through the filter and expel it out of the chimney of the lorica. To explore such a pumping mechanism we replace the flagellum in the CFD model with a $b = 5$-μm-wide sheet that spans almost the entire width of the filter (Movies S3–S5). The time-averaged CFD flow agrees well with the flow observed for *D. grandis* (Fig. 3). The model leads to the time-averaged flagellum force in the z-direction $F_5 = 12.1$ pN, the time-averaged power $P_5 = 2.20$ fW, and the clearance rate $Q_5 = 898\ \mu m^3 \cdot s^{-1}$, slightly lower than the experimentally observed clearance rate.

To explore the vane-based pumping mechanism conjecture for other choanoflagellates we make a rough estimate of the clearance rate as the volume flow rate given by the simple model

$$Q_V = AW\lambda f, \qquad [5]$$

where W is the diameter of the chimney of the lorica and λ the flagellar wavelength. We assume that the flagellum is moving in the central beat plane with amplitude A and that the flagellar vane is attached to filter and chimney. The average peak-to-peak amplitude of the flagellar vane must therefore be A, and we assume that a water volume $AW\lambda$ is forced through the filter and out of the chimney per flagellar beat period. For *D. grandis* we find the estimate $Q_V = (1.41 \pm 0.50) \cdot 10^3\ \mu m^3 \cdot s^{-1}$ in good agreement with the clearance rate based on the observed flow field (Table 1).

In fact, Q_V provides a solid prediction of the observed clearance rate Q in six of the seven species for which the naked flagellum clearance rate estimate Q_T cannot account for Q (Table 1). Thus, two species seem to use a simple flagellum to drive the feeding current, whereas six choanoflagellate species and the choanocyte rely on a flagellar vane. A narrow vane has been observed in *Monosiga brevicollis*, but a vane this small would have only limited influence on the clearance rate (Fig. S5), and the apparent discrepancy is certainly within estimate uncertainties. Only for *Codosiga botrytis* does neither of the two models adequately predict Q. This species has a long and rapidly beating flagellum that extends far beyond the collar and also the finest of the choanoflagellate filters. Combined, this suggests that this species may not perform actual filter feeding, but instead relies on cross-flow filtration in which the flow passes along and not through the filter. The suggested pumping mechanism would also provide a means to avoid unwanted filter circumvention in loricate as well as nonloricate species. If the vane spans most of the collar width, a flagellum wavelength "traps" a package of water that has to be expelled with the flagellar beat. Furthermore, typical flagellar beat frequencies of eukaryotic organisms are in the range 30–70 Hz (1, 18), and the low beat frequencies found in *D. grandis* and a number of other choanoflagellate species stand out (Table 1). We speculate that the low beat frequencies are the result of extensive flagellar vanes and their high force requirements. While the dynein motor proteins themselves would easily

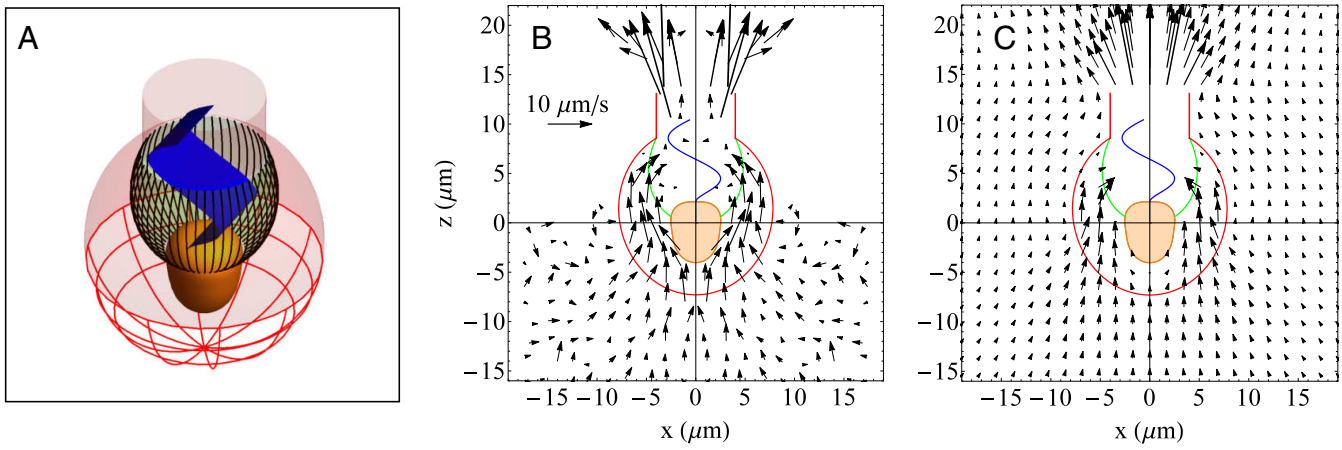

Fig. 3. Model morphology with a flagellar vane, observed average velocity field for *D. grandis*, and velocity field from CFD model including a 5-μm-wide flagellar vane. (*A*) The model morphology shows the cell (orange), the collar filter (green), the flagellum with a 5-μm-wide flagellar vane (blue), and the lorica (red). (*B*) Observed average velocity field. The velocity field is identical to the velocity field in Fig. 2*B*, and it is shown repeatedly to facilitate comparison with the CFD result. (*C*) The CFD velocity field in the *xz* plane is time averaged over the flagellar beat cycle, and the velocity vectors inside filter and chimney are omitted for clarity. The CFD model with a flagellar vane predicts a feeding flow in through the permeable lower part of the lorica and a clearance rate in good agreement with the experimental observations for *D. grandis*.

provide the needed force (31), the shear due to the flagellar beat motion could be too much for delicate vane structures. The presence of a 5-μm-wide vane increases the energetic costs of beating the flagellum by an order of magnitude, making the energetic costs a significant fraction of the total energy budget of the cell, contrary to common belief (32, 33). This is in agreement with results from the similar choanocytes (34) and demonstrates a strong trade-off for microbial filter feeders between acquiring new energy and investing energy to do so.

The Filter-Feeder Trade-Off and the Optimum Filter. The main purpose of the filter is to intercept as much food as possible. The above-mentioned filter trade-off suggests that there is an optimum filter spacing that will maximize the prey encounter rate E in terms of prey biomass per unit time. The encounter rate can be expressed as the integral

$$E = Q \int_0^\infty \beta(s)\, C(s)\, \mathrm{d}s, \qquad [6]$$

where β is the collection efficiency, C the size-specific mass concentration of prey particles, and s the particle diameter. It is generally accepted that logarithmic particle size bins contain approximately equal amounts of biomass (35),

$$C(s) = \frac{C_0/\ln 10}{s}, \qquad [7]$$

where C_0 is the particle mass concentration within each decade in particle diameter. Now, if the particles are captured by sieving, we can assume 100% collection efficiency, $\beta = 1$, for particles with diameter greater than the filter gap $l - 2a$ and smaller than the maximum prey size d. In this case we can write the encounter rate as

$$\begin{aligned} E &= Q \int_{l-2a}^{d} C(s)\mathrm{d}s \\ &= E_0 \langle \kappa \rangle \log \frac{d/a}{l/a - 2}, \end{aligned} \qquad [8]$$

where $E_0 = (a/\mu) F C_0$ is independent of l and d. Independent of the flagellum force F and method of pumping, it is thus possible to predict the optimum filter spacing of aquatic microbial filter feeders. With the maximum prey size $d = (1/3)\,\mathrm{ESR} = 0.93\ \mu\mathrm{m}$ for *D. grandis* (approximately the openings of the coarse outer filter), we obtain the optimum dimensionless filter spacing $l/a = 8.4$ in close agreement with the observed average value (Fig. 4*A*). The optimum filter spacing increases approximately linearly with the maximum prey size in the range relevant for choanoflagellates, and it is consistent with observations (Fig. 4*B*). One species, *C. botrytis*, deviates from this pattern, consistent with our suggestion that this species may not be a true filter feeder. We can approximate the encounter rate when $l/a \gg 1$ as

$$E \approx E_0 \frac{l/a}{8\pi} \left(1 - 2\ln\frac{2\pi}{l/a}\right) \log\frac{d/a}{l/a}, \qquad [9]$$

which allows analytical determination of the optimum filter spacing

$$\frac{l}{a} \approx \exp\left[-1 + \frac{1}{\ln(d/a)} + \frac{\ln(2\pi) - 1/2}{[\ln(d/a)]^2}\right] \frac{d}{a}. \qquad [10]$$

The expression shows that the optimum filter spacing is approximately proportional to the maximum prey size when the filter spacing is large, leading to a relatively small prey size range. Particles smaller than the filter spacing can be collected by direct interception or diffusional deposition, but these effects are estimated to be small compared with sieving for the measured filter spacing of *D. grandis* (36).

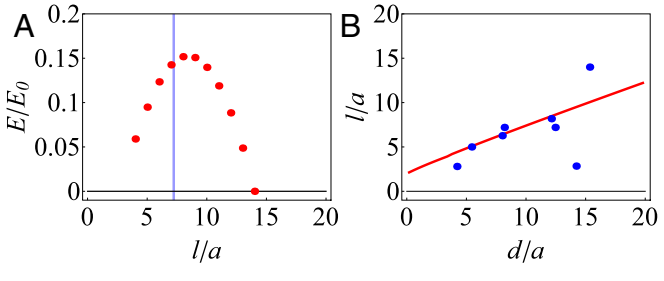

Fig. 4. Optimum choanoflagellate filters. (*A*) Encounter rate as function of dimensionless filter spacing (Eq. **8**). The vertical line (blue) indicates the observed average of the dimensionless filter spacing. (*B*) The theoretical prediction for the optimum dimensionless filter spacing (solid line, red) and the observed dimensionless filter spacing for the choanoflagellates in Table 1 (solid circles, blue) as functions of the maximum dimensionless prey diameter. We have assumed that the maximum prey diameter is equal to (1/3) ESR. The outlier below the predicted line is *C. botrytis*, speculated to rely on cross-flow filtration rather than true filtration.

Conclusion

We have shown that a simple, naked flagellum cannot account for the clearance rates observed in many choanoflagellate species. Instead, we suggest a widespread presence of the sporadically observed flagellar vane. The proposed pumping mechanism is radically different and can explain how choanoflagellates can perform efficient small-scale filter feeding. The explored problems and our model estimates are relevant to the understanding of small-scale filtering in general, and the mechanistic insights allow quantification of the trade-offs involved in various microbial feeding modes. We have, for instance, demonstrated that microbial filter feeding is an energetically costly process that takes up much more than a few percent of the total energy budget of the cell as otherwise typically believed.

Materials and Methods

Experimental Organisms. The choanoflagellate *D. grandis* (American Type Culture Collection no. 50111) was grown nonaxenically in the dark in B1 medium (salinity 32) at 10 °C. The culture was diluted once every 2–3 wk, and a few organically grown, autoclaved, rice grains were added per 65-mL flask to serve as bacterial substrate.

Videography of Flagellum Motion and Feeding Flow. To explore the near-cell flow field and the motion of the beating flagellum, cells were observed at high magnification, using a high-speed digital video. An Olympus IX-71 inverted microscope equipped with a UPLSAPO60XO/1.35 oil-immersion objective and a U-ECA magnifying lens provided a total of 1,920× magnification. Video sequences were obtained using a Phantom v210 high-speed digital video system. Videos were recorded at a frame rate of 100 fps and a resolution of 1,024 pixels × 800 pixels. This provided 10 pixels/μm. Observations were done in an ≈1-mL chamber, constructed as a 5-mm-high polycarbonate ring (diameter 2 cm) mounted with silicone between an objective slide and a cover glass. Cells either were free swimming or settled onto the slide. Flagellum length and average amplitude of the flagellar beat were estimated on five individuals that were oriented with the flagellum beat plane aligned with the focal plane of the microscope. For each frame in a single beat cycle, the flagellum position was digitized manually using ImageJ by identifying approximately 15 points along the flagellum. Neutrally buoyant, 300-nm polystyrene beads were added to a concentration of $\sim 1 \cdot 10^6$ mL^{-1} to visualize the water flow. The particles were pretreated with BSA and sonicated before use to avoid clumping.

Flow-Field Analysis. Based on cell alignment, a total of 19 video sequences, each fielding a unique individual, were selected for use in the flow-field analysis. The frequency of the flagellar beat was noted at 1-s intervals, by manual, visual inspection of the slowed-down 100-fps video sequences. Two-dimensional particle tracks were resolved on reduced–frame-rate video sequences (10 fps), using the manual tracking plugin for ImageJ. A total of 73 tracks were used to construct the velocity field. Each particle track was associated with the frequency of the flagellar beat at the corresponding time. All particle tracks were collated using the average model morphology,

and the velocity field in the *xz* plane was constructed using a square grid with 2-μm $\times$ 2-μm spatial resolution. The velocity field was assumed to have rotational symmetry about the longitudinal axis of the cell, and the observed velocity field in the *xz* plane was therefore correspondingly assumed to have left–right reflection symmetry with respect to the longitudinal axis. Within each grid window the manually detected particle positions were selected and for each particle track the average particle position and velocity were determined. Position and velocity associated with a given grid window were subsequently determined as the equally weighted average over all particle tracks within the window.

ACKNOWLEDGMENTS. We thank Jasmine Mah for providing videos of *M. brevicollis* and Øjvind Moestrup and Helge Abildhauge Thomsen for helpful discussions. The Centre for Ocean Life is a Villum Kann Rasmussen Centre of Excellence supported by the Villum Foundation, and S.S.A. and J.H.W. were supported by a research grant (9278) from the Villum Foundation.

1. Fenchel T (1982) Ecology of heterotrophic microflagellates. I. Some important forms and their functional morphology. *Mar Ecol Prog Ser* 8:211–223.
2. Fenchel T (1984) Suspended marine bacteria as a food Source. *Flows of Energy and Materials in Marine Ecosystems*, ed Fasham MJR (Plenum, New York), pp 301–315.
3. Kiørboe T, Plough H, Thygesen UH (2001) Fluid motion and solute distribution around sinking aggregates. I. Small-scale fluxes and heterogeneity of nutrients in the pelagic environment. *Mar Ecol Prog Ser* 211:1–13.
4. Kiørboe T (2011) How zooplankton feed: Mechanisms, traits and trade-offs. *Biol Rev* 86:311–339.
5. Fenchel T (1986) Protozoan filter feeding. *Prog Protistology* 1:65–113.
6. Larsen PS, Riisgård HU (1994) The sponge pump. *J Theor Biol* 168:53–63.
7. Riisgård HU, Larsen PS (2010) Particle capture mechanisms in suspension-feeding invertebrates. *Mar Ecol Prog Ser* 418:255–293.
8. Fenchel T (1980) Relation between particle size selection and clearance in suspension-feeding ciliates. *Limnol Oceanogr* 25:733–738.
9. Ayaz F, Pedley TJ (1999) Flow through and particle interception by an array of closely-spaced circular cylinders. *Eur J Mech B Fluids* 18:173–196.
10. Pettitt ME, Orme BAA, Blake JR, Leadbeater BSC (2002) The hydrodynamics of filter feeding in choanoflagellates. *Eur J Protistol* 38:313–332.
11. Leadbeater BSC (2015) *The Choanoflagellates: Evolution, Biology and Ecology*. (Cambridge Univ Press, Cambridge, UK).
12. Lapage G (1925) Notes on the choanoflagellate, *Codosiga botrytis*, ehrbg. *J Cell Sci* 69:471–508.
13. Andersen P (1988/1989) Functional biology of the choanoflagellate *Diaphanoeca grandis* Ellis. *Mar Microb Food Webs* 3:35–50.
14. Roper M, Dayel MJ, Pepper RE, Koehl MAR (2013) Cooperatively generated stresslet flows supply fresh fluid to multicellular choanoflagellate colonies. *Phys Rev Lett* 110:228104.
15. Dayel MJ, King N (2014) Prey capture and phagocytosis in the choanoflagellate *Salpingoeca rosetta*. *PLoS One* 9:e95577.
16. Kirkegaard JB, Goldstein RE (2016) Filter-feeding, near-field flows, and the morphologies of colonial choanoflagellates. *Phys Rev E* 94:052401.
17. Hibbert DJ (1975) Observations on the ultrastructure of the choanoflagellate *Codosiga botrytis* (ehr.) Saville-Kent with special reference to the flagellar apparatus. *J Cell Sci* 17:191–219.
18. Sleigh MA (1964) Flagellar movement of the sessile flagellates *Actinomonas, Codonosiga, Monas*. *J Cell Sci* 105:405–414.
19. Eccleston PJD, Leadbeater BSC (1994) A comparison of the growth kinetics of 6 marine heterotrophic nanoflagellates fed with one bacterial species. *Mar Ecol Prog Ser* 105:167–178.
20. Mah JL, Christensen-Dalsgaard KK, Leys SP (2014) Choanoflagellate and choanocyte collar-flagellar systems and the assumption of homology. *Evol Dev* 16:25–37.
21. Boenigk J, Arndt H (2000) Comparative studies on the feeding behavior of two heterotrophic nanoflagellates: The filter-feeding choanoflagellate *Monosiga ovata* and the raptorial-feeding kinetoplastid *Rhynchomonas nasuta*. *Aquat Microb Ecol* 22:243–249.
22. Leadbeater BSC (1972) Fine-structural observations on some marine choanoflagellates from the coast of Norway. *J Mar Biol Assoc UK* 52:67–79.
23. Moestrup Ø (1982) Flagellar structure in algae: A review, with new observations particularly on the Chrysophyceae, Phaeophyceae (Fucophyceae), Euglenophyceae, and *Reckertia*. *Phycologia* 21:427–528.
24. Keller JB (1964) Viscous flow through a grating or lattice of circular cylinders. *J Fluid Mech* 18:94–96.
25. Tamada K, Fujikawa H (1957) The steady two-dimensional flow of viscous fluid at low Reynolds numbers passing through an infinite row of equal parallel circular cylinders. *Q J Mech Appl Math* 10:425–432.
26. Berg HC (1993) *Random Walks in Biology* (Princeton Univ Press, Princeton).
27. Leadbeater BSC (2006) The 'mystery' of the flagellar vane in choanoflagellates. *Nova Hedwigia Beiheft* 130:213–223.
28. Mehl D, Reiswig HM (1991) The presence of flagellar vanes in choanomeres of Porifera and their possible phylogenetic implications. *J Zool Syst Evol Res* 29:312–319.
29. Weissenfels N (1992) The filtration apparatus for food collection in freshwater sponges (Porifera, Spongillidae). *Zoomorphology* 112:51–55.
30. Jaffrin MY, Shapiro AH (1971) Peristaltic pumping. *Ann Rev Fluid Mech* 3:13–37.
31. Lindemann CB (2003) Structural-functional relationships of the dynein, spokes, and central-pair projections predicted from an analysis of the forces acting within a flagellum. *Biophys J* 84:4115–4126.
32. Purcell EM (1977) Life at low Reynolds number. *Am J Phys* 45:3–11.
33. Guasto JS, Rusconi R, Stocker R (2012) Fluid mechanics of planktonic microorganisms. *Annu Rev Fluid Mech* 44:373–400.
34. Leys SP, et al. (2011) The sponge pump: The role of current induced flow in the design of the sponge body plan. *PLoS One* 6:e27787.
35. Sheldon RW, Prakash A, Sutcliffe Jr. WH (1972) The size distribution of particles in the ocean. *Limnol Oceanogr* 17:327–340.
36. Spielman LA (1977) Particle capture from low-speed laminar flows. *Ann Rev Fluid Mech* 9:297–319.
37. Pozrikidis C (2011) *Introduction to Theoretical and Computational Fluid Dynamics* (Oxford Univ Press, Oxford), 2nd Ed.
38. Happel J, Brenner H (1983) *Low Reynolds Number Hydrodynamics: With Special Applications to Particulate Media* (Martinus Nijhoff, The Hague, The Netherlands).